Applied Nanoscience (2018) 8:1649–1668
https://doi.org/10.1007/s13204-018-0837-2

ORIGINAL ARTICLE

Silica nanocomposites based on silver nanoparticles-functionalization and pH effect

M. Zienkiewicz-Strzałka[1] · A. Deryło-Marczewska[1] · R. B. Kozakevych[2]

Received: 21 March 2018 / Accepted: 3 July 2018 / Published online: 12 July 2018

Abstract
Current reports in the field of nanotechnology indicate that the properties of metal nanoparticles are determined by their features such as size, shape, composition as well as a degree of crystallinity and stability. These, in turn, may depend heavily on their preparation way, treatment during and after synthesis and finally on properties of the supports and matrices. The goal of presented work was to determine the shape, size, and distribution of silver nanoparticles depending on preparation conditions. In particular, the issues of the formation of silver nanostructures (AgNP) with various shapes and sizes depending on functionalized silica surface as well as on the conditions of the impregnation step by noble metal ions (especially pH) were considered. In particular, the comprehensive approach to determine the impact of pH conditions on the properties of metallic nanoparticles is laid down in this work. Three types of fumed silica materials were selected as the supports of silver nanostructures (Aerosil 150, Aerosil 300 and Silochrom C-120). Silica materials were chemically functionalized by thiol and amine groups and treated with diamminesilver(I) ions $[Ag(NH_3)_2]^+$. As a result of their reduction silicas adorned with silver nanostructures were obtained. In this work, the AgNP in the form of very small nanoparticles, longitudinal and spherical forms and greater structures with nondescript shape were successfully received and characterized through changing the form of functional groups on the solid surface by adjusting the pH conditions. It turns out that protonation and deprotonation of thiol, amino, and hydroxyl groups can be responsible for possible interactions between noble metal ions and functional groups in the form of both attractive and repulsive electrostatic interactions. The Ag nanoparticle/silica nanocomposites were investigated by X-ray diffraction, atomic force microscopy, potentiometric titration and X-ray photoelectron spectroscopy.

Keywords Silver nanoparticle · Size control · Fumed silica · Impregnation · Ammine complex

Introduction

Functionalization of the support surface is often a precondition for many potential applications when the interactions between components can affect the stability of nanoparticles and colloids (Haddada et al. 2013; Milczarek et al. 2014). Surface functionalization of the most useful matrixes leads to incorporation of the active groups on the external layers and thus formation of the active sites with affinity to bind other molecules, biomolecules, and noble metal nanoparticles. The bonding forces between the unmodified surface and other components are often too weak to obtain stable composites and conjugates. The incorporation of the functional groups with high affinity to the considered matrixes can be responsible for changing and replacing the undesirable weaker bound ligands, which are or may be present after their synthesis or prior treatment. In practical applications of functionalization process, the conditions of functionalization, modification, and preparation of desirable materials should be carefully optimized. The amino- and thiol-functionalized nanoparticles are quite important in the field of commercial composite materials (Minsoo 2008; Chang et al. 2008), catalysts (Penkova et al. 2009; Wang and Shantz 2010; Suzuki et al. 2008), medical diagnostics (Ashtari et al. 2005), and biochemistry (He et al. 2007; Curran et al. 2005; Chen et al. 2006) and many others (Chiron et al. 2003; Mercier and Pinnavaia 1998; Brown et al. 2000; Yang et al.

✉ M. Zienkiewicz-Strzałka
gosiazienkiewicz@wp.pl

[1] Department of Physicochemistry of Solid Surface Faculty of Chemistry, Maria Curie-Skłodowska University, sq. Maria Curie-Sklodowskiej 3, 20-031 Lublin, Poland

[2] Chuiko Institute of Surface Chemistry, National Academy of Sciences of Ukraine, 17 Generala Naumova St., Kiev 03164, Ukraine

2013). Many of these unique and valuable properties are influenced strongly by the experimental conditions during formation and applications (Cao 2004; Giri et al. 2011; Yeo et al. 2003; Zhang et al. 2004, 2006, 2013; Chimentao et al. 2004; He et al. 2004; Yang et al. 2013; Love et al. 2005; Gittins and Caruso 2002; Katz and Willner 2004).

Nanoparticles are important scientific tools in many areas with large and still growing practical importance (Bindhu and Umadevi 2014; Elechiguerra et al. 2005; Uchihara 2007; Galiano et al. 2008). An important advantage of the creation of silver nanoclusters embedded in a solid matrix is improving the stability of silver nanoparticles and the reduction of a silver amount in comparison to pure silver coatings resulting in lower toxicity. Some examples include the attempts to produce antibacterial coatings containing metallic silver nanoclusters embedded in a silica matrix as screens, covers, and microphone felt (Miola et al. 2014). Properties and usefulness of nanoparticles are determined in the same way by the composition and size as their stability and accessibility. Certain, important properties of the matter are not available for bulk solids or isolated molecules (Ju-Nam and Lead 2008; Sharma et al. 2009). An antibacterial silica composite coating with silver nanoclusters was deposited on a commercial polymer suitable for aerospace application (Balagna et al. 2012), employed as a sensing element for recognition the cancer cells (Ferraris et al. 2011) and devices for protein detection (Ohtsuki et al. 2010). The large group of functional materials includes also the polymer/silver composites as a biodegradable poly(ethylene oxide) nanofibers containing silver nanoparticles as biomaterials (Kim et al. 2009). Nowadays, at least two basic ways of surface functionalization in relation to nanoparticles are possible: functionalization of the nanoparticle surface and modification of solid surfaces and matrices by nanoparticles. As first, surface modification of nanoparticles by incorporation of various ligands (Sakura et al. 2005; Stenkamp et al. 2001; Zhao et al. 2005; Liu et al. 2008), functional groups (Hiramatsu and Osterloh 2004; Sarathy et al. 1997) and many others species (Wang et al. 2002; Thompson et al. 2008) onto nanoparticle surfaces is considered. This approach determines the interaction between modified nanoparticles, environment and biosystems as well as allows to control the growth of the particles and prevents their aggregation and precipitation. On the other hand, noble metal nanoparticles can be incorporated into solid support by integration with carrier surface decorated by specific functional groups as amine or thiol species (Dharanivasan et al. 2015). The possible mechanisms of the formation of such hybrid materials and biomolecule conjugates include:

- *The chemisorption nature of interactions* by ligand binding with the surface. Here the thiol or amine groups can be considered as an example. The explanation of this phenomena assumes the binding by the donation of electron density from the functional group into the metal nanoparticle according to heterolytic fission.
- *Electrostatic interactions* The interactions occur between positively and negatively charged components. As an example, the electrostatic binding phenomena may occur in protein–nanoparticle interactions (Forest et al. 2015).
- *Binding by conjugation according to the creation of covalent bonds* through functional groups on both components.
- *Non-covalent interactions* with receptor–ligand systems.

Quite often the nature of the interaction is not clearly defined, and the apparent effect being a consequence of several different effects should be considered, especially in the nanoparticles-to-biological system interactions. The potential applications require clarifying the relationship between the properties of the components. The composition of nanoparticles (Sohaebuddin et al. 2010; Gojova et al. 2007), their hydrophobicity (Turci et al. 2010), presence or absence of functional groups and finally pH, ability to agglomerate and changes in the surface energy have been shown to affect such interactions.

In this work, we tried to determine the relationship between shape, size, and distribution of silver nanoparticles deposited on silica surface and preparation conditions, types of functionalized silica surface as well as on conditions of the impregnation step by noble metal ions (especially pH). Especially, the problem how surface properties (forms of functional groups on the surface) influence the formation of the noble metal nanostructures was developed in this work. The influence of pH on the aggregation and size of various types of nanoparticles synthesized by different methods and the importance of this phenomena was indicated initially in the literature (Weisbecker et al. 1996). However this problem is not investigated enough, especially taking into account the application meaning. Thus far, size, shape, and surface properties of nanoparticles have all been indicated as exerting influence on the other biomolecules. This seems to be the significant reason for the advisability of research over the impact of the synthesis parameters and the properties of obtained nanomaterials.

Experimental

Materials

Pyrogenic silica materials as a hydrophilic fumed silica AEROSIL® 150 (Asil150) and AEROSIL® 300 (Asil 300) were purchased in Evonik Degussa GmbH, Germany. Silochrom sample was prepared by hydrothermal treatment of AEROSIL® 200 sample by mixing with water for obtaining a homogeneous mixture. The suspension was allowed

to gelation and obtained hydrogel was crushed and dried at 120 °C for 12 h. The final sample was calcined at 600 °C over 5 h under in air atmosphere.

Surface functionalization of pyrogenic silica samples by thiol and amine groups was achieved using a post-grafting process. For obtaining thiol- and amine-functionalized materials, 3.0 g of the support were placed in a round-bottom flask with 50 mL of toluene and an appropriate amount of (3-aminopropyl) triethoxysilane (APTES, purchased from Sigma-Aldrich) or (3-mercaptopropyl) trimethoxysilane (MPTMS, Sigma-Aldrich). The amount of silane coupling agent (APTES or MPTMS) was calculated for the half monolayer and close to full monolayer formation by thiol and amine functional groups (0.3 and 0.6 mmol/g, respectively). The resultant mixtures were stirred and refluxed at 150 °C for 2 h. Finally, the materials were washed with ethanol and vacuum dried at 120 °C for 12 h to obtain functionalized pyrogenic silica samples. The synthesis procedures of functionalized silica samples are shown in Fig. 1.

Diamminesilver(I) complex $[Ag(NH_3)_2]^+$was freshly prepared in the laboratory due to its short shelf life. It was prepared by dissolving silver(I) oxide in concentrated ammonia as follows: silver nitrate (0.3 mol/L) (Sigma-Aldrich ≥ 99.0%) was mixed with sodium hydroxide aqueous solution (1.25 mol/L) for obtaining a brown precipitate of Ag_2O. 1 g of as-prepared silver(I) oxide was separated from the solution, washed with distilled water and dissolved in 2.63 mL of concentrated (25%) ammonium hydroxide giving diamminesilver(I) complex solution.

The silver ions deposition on functionalized SiO_2 samples were carried out by the following procedure. First, two types of solutions with pH 3 and pH 8 were prepared by addition of appropriate amount of HNO_3 or NH_4OH to distilled water. Functionalized silica samples (0.25 g) were added to solutions (10 mL) with pH 3 and pH 8. Finally, the diamminesilver(I) solution (0.037 g) was added to the prepared mixtures for obtaining the initial concentration of silver ions at the level of 10% relative to the silica material. The mixtures were placed in an incubator and stirred overnight with stirring rate of 90 rpm. After impregnation white powders were separated from the solution, gently washed with distilled water and thermally treated with temperature ramping from r.t. to 300 °C in the muffle furnace by 1 h. As a result of the performed work, the series of colored (brown, dark brown and dark grey) powders were obtained.

Measurements and calculations

The surface charge properties were experimentally determined by potentiometric titration of the suspension at constant temperature 25 °C maintained by the thermostatic device. In experiments 30 cm^3 of 0.1 mol/dm^3 NaCl as an electrolyte was used. The initial pH was established by addition of 0.3 cm^3 of 0.5 mol/dm^3 HCl. The equilibration time of initial pH was attained under inert gas conditions by 2 h and any drifting at the start of the titration was not observed. The 0.2 mol/dm^3 NaOH solution was used as a titrant, added gradually using automatic burette Dosimat 665 (Metrohm, Switzerland) controlled by a custom PC program coupled with a digital pH-meter pHm-240 (Radiometer, Copenhagen); Radiometer pH-standards were also used as pH reference. Prior to potentiometric titration measurements, the solid samples were dried by 24 h at 120 °C. The problem of CO_2 contamination was avoided by operation under the nitrogen atmosphere. Textural properties of initial and functionalized materials were obtained by measuring N_2 adsorption/desorption isotherms at − 196 °C over the full range of relative pressures, using a Micromeritics ASAP2020 equipment. Specific surface areas (S_{BET}) were estimated from experimental isotherms by applying the Brunauer–Emmett–Teller (BET) theory. Pore size distribution curves were obtained from the adsorption branch using

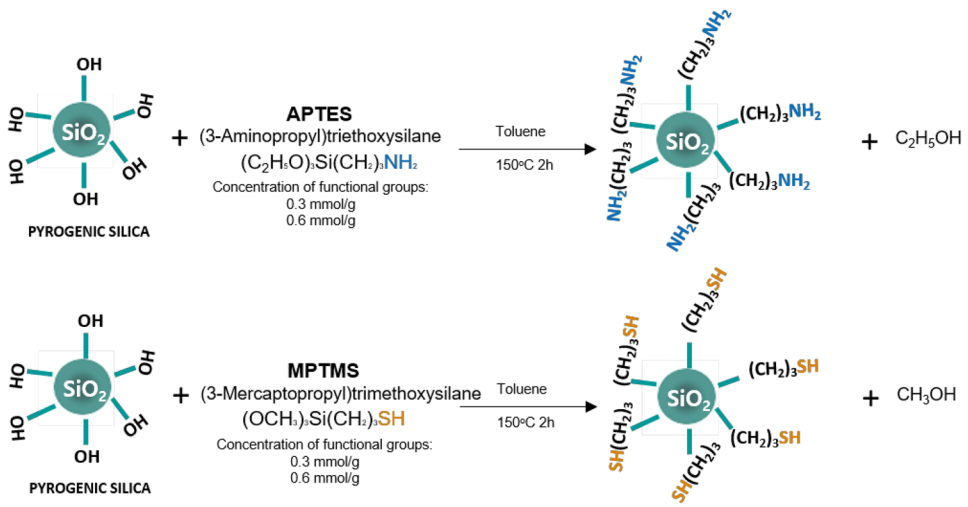

Fig. 1 Schematic diagram of synthesis of amine- and thiol-functionalized pyrogenic silica samples

the Barrett–Joyner–Halenda (BJH) model with cylindrical pores as well as and non-local density functional theory (NLDFT) method using cylinder pore geometry. All samples were outgassed before analysis at 120 °C for 24 h in degas port of analyzer. The obtained silver/silica composites were characterized by X-ray diffraction (XRD) using Empyrean diffractometer (PANalytical) with CuKα radiation ($\lambda = 1.5418$ Å) in the wide range of diffraction angles from 10° to 70° of 2θ. The size of silver crystallites was determined from the full width at half maximum (FWHM) of X-ray diffraction peaks by Scherrer equation applying width of the X-ray lines (Cullity 1978). The fitting procedure of experimental patterns was performed by WAXSFIT Software (Rabiej 2014). Atomic force microscopy (AFM) analysis was performed using Bruker-Veeco-Digital Instruments Multi-Mode Atomic Force Microscopes in AFM Tapping Mode. For each sample, several regions were investigated to representative results and confirm the homogeneity of particle deposition on the silica surface. The measurements were done using Antimony n-doped Si cantilever TAP150A with force constant $k = 5$ N/m and resonance frequency $f_0 = 150$ kHz. Analysis of the AFM data was performed by NanoScope Analysis software from Bruker. X-ray photoelectron spectroscopy (XPS) analysis was obtained by Multichamber ultra-high vacuum (UHV) System, Prevac (2009). Transmission electron micrographs were obtained from a Titan G2 60-300 (FEI) operating at 200 kV. Scanning electron micrographs were collected from Quanta 3D FEG (FEI).

Results and discussion

Surface properties: isoelectric point and surface charge density

The properties of surfaces and interfaces of supports and solid matrices play an important role in the properties and behavior both in preparation and in the application stage. It should be noted that surface of many mineral oxides can change when they are exposed to the external environment and other substances during their modification and doping. The experimental investigation of the surface properties such as surface charge densities of functionalized pyrogenic silica seems to be appropriate and valuable for investigating how surface properties (forms of functional groups on the surface) influence the formation of the noble metal nanostructures. Pyrogenic silica materials were characterized by potentiometric titration for describing their surface properties before and after functionalization. Figure 2 shows the schematic model of functionalization with the changes of the surface properties and summarizes our findings in this part of a research. More importantly, the range of pH in which the positive or negative charge appears, allow to confront the silver ions with the surface of a specified charge and identify the impact of this parameter on the size, shape, and population of the silver nanoobjects (Fig. 3).

Figure 4 shows the set of potentiometric titration curves, and surface charge density for initial Silochrom, Asil150 and Asil 300 silicates as well as their comparison with potentiometric titration curve for a blank sample (background electrolyte). For initial silica samples, the isoelectric point was found to be at around 3 in all cases. This value is close to that reported in the literature (Kosmulski 2002; Farooq et al. 2011). The pH dependence of the surface charge is presented in Fig. 5. In the case of amine-functionalized samples, the significant shift of the PZC to the higher pH values after functionalization was observed for all cases (Fig. 5a–c). The pH_{PZC} increases with increasing number of ammine groups from pH_{PZC} 3 for initial silica samples to close to 8.5 and even up to 9 when the amount of amine groups attains 0.3 and 0.6 mmol/g, respectively. The shift of pH_{PZC} unambiguously illustrates that modification of the silica surface by silylation causes that SiO_2–OH species interacted with the NH_2 group. It is conceivable that small part of silanol groups remained in an initial state due to the lower value of an isoelectric point for investigated sample compared with pure APTES (pH_{PZC} 10.5). The actual results show that the surface modification by amine groups is clearly reflected in the PZC properties. The amine groups on the surface generate a basic properties on the porous silica materials. Potentiometric titration results of thiol-functionalized pyrogenic silica samples suggest that the significant changes and shifts of surface charge after modification were not clearly marked. All samples remained positive charged at low pH values (below pH 3) and negatively charged at higher pH with a plateau from pH 3.5 to 6. Lack of changes in the position of PZC may be related to very similar acidic properties of thiol group and silanols.

Structural studies of the silica/AgNP composites

Aerosil grades of silica are porous materials, with a few of nanopores. The porosity of investigated samples was described based on low-temperature N_2 adsorption/desorption isotherms. Obtained results illustrate and explain the effect of surface functionalization from the perspective of the porous structure. The shape of reversible experimental isotherms, both of the pristine fumed silicas and modified samples, corresponding to the II type of the classification of isotherms (Broekhoff 1979; Sing et al. 1985). The presence of modifying factors significantly reduces the available surface of the nanomaterials. The S_{BET} of initial fumed silica materials were estimated as 262, 144 and 106 m^2/g for Asil300, Asil150, and Silochrom, respectively. Amine-functionalization resulted decreasing the S_{BET} by 44, 15 and

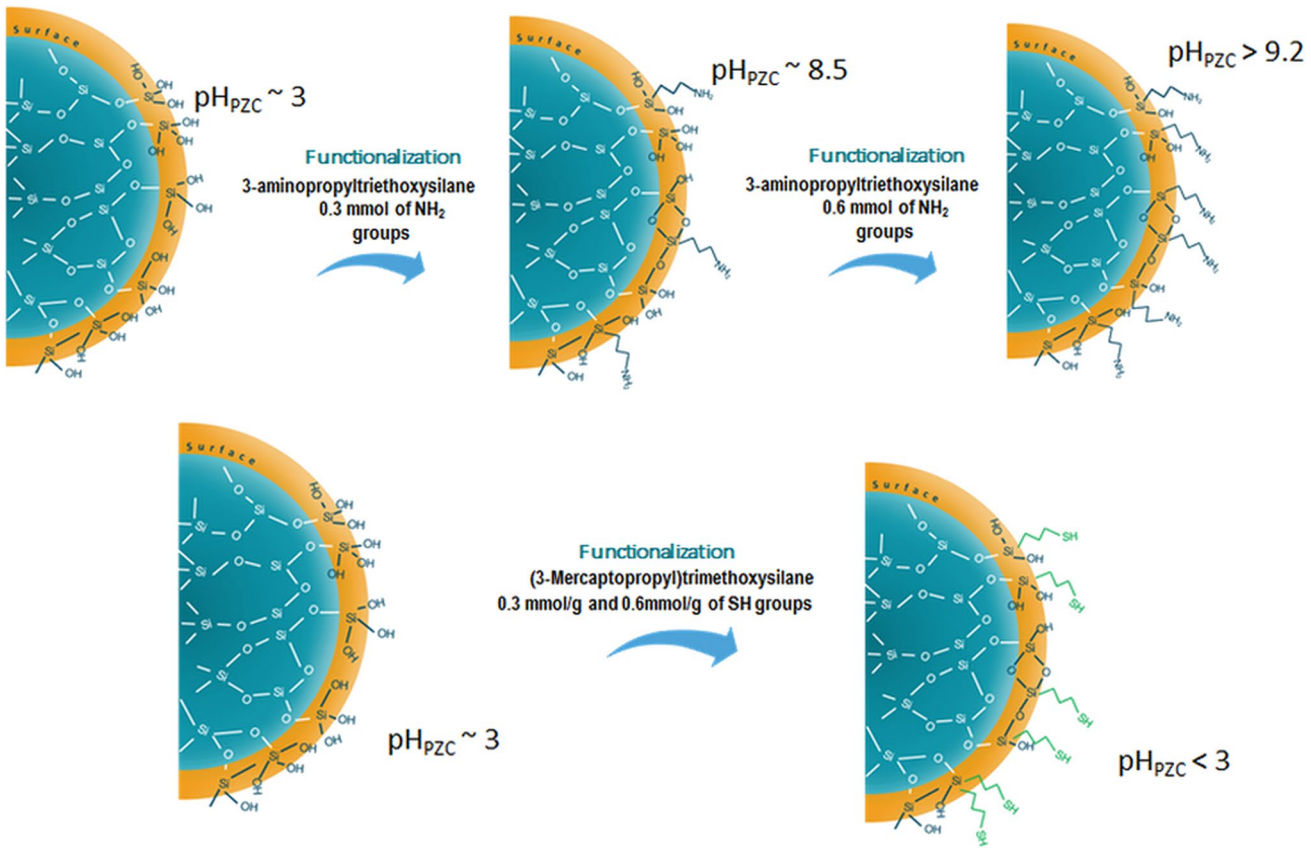

Fig. 2 Model of amine- and thiol-functionalized pyrogenic silica surface and changes of the surface charge after incorporation various amount of functional groups

14.6% for the above samples. The same direction of changes has been preserved when the silver nanoparticles were incorporated onto silica. Then, the S_{BET} is further reduced by 75, 54, and 14.6%, respectively, in relation to the primary values. The effect of physical blocking the silica porous structure by modifying elements (especially silver nanoparticles) was confirmed by analysis of the pore size distributions. In all cases, it was observed the change of the number of nanopores and mesopores, whereas their average sizes were very similar (~2 and 40 nm).

The microstructure of investigated silver/silica composites was evaluated by powder X-ray diffraction. Figure 6 shows experimental XRD patterns for all samples. The XRD patterns obtained for the silver–silica composites show similar behavior for all types of silica. Figure 6 shows that the SiO_4 tetrahedrons of pyrogenic silica samples have an irregular arrangement confirmed by the absence of defined crystalline X-ray diffraction reflections from silica phase. It shows only broad, well-marked amorphous halo diffraction peak at 2θ of 22° corresponding to an amorphous SiO_2 structure.

Only for some of the samples (initial samples and silicates modified by amine groups), the XRD patterns clearly confirmed the crystalline structure of silver nanoparticles. The wide-angle XRD patterns reveal the presence of intense diffraction peaks which correspond to the Ag(111), Ag(200), Ag(220) lattice planes of the cubic structure of silver phase (JCPDS no. 4-0783). The lattice constant has been found to be $a = 0.41$ nm, which is consistent with the standard value $a = 0.41$ nm. Thus, the identification of the silver nanostructures at this step was only possible in the case of non-functionalized materials and materials modified by amine groups for both pH values. It is worth noting that no peaks of other impurity crystalline phases like oxides or chlorides have been detected. The detailed analysis of the diffraction peaks, in terms of full width at half maximum, allow to investigate the size and indirectly shape of the silver crystallites. The nanocrystallite size L was calculated as a function of peak width by Scherrer equation:

$$L = \frac{k\lambda}{\beta \cos \Theta}, \quad (1)$$

where k is a constant related to crystallite shape. In this case, k equals 0.9. λ is the X-ray wavelength and equals 1.5418. Θ peak position in radians. β is full width at half maximum of peaks located at any 2θ in the pattern corrected

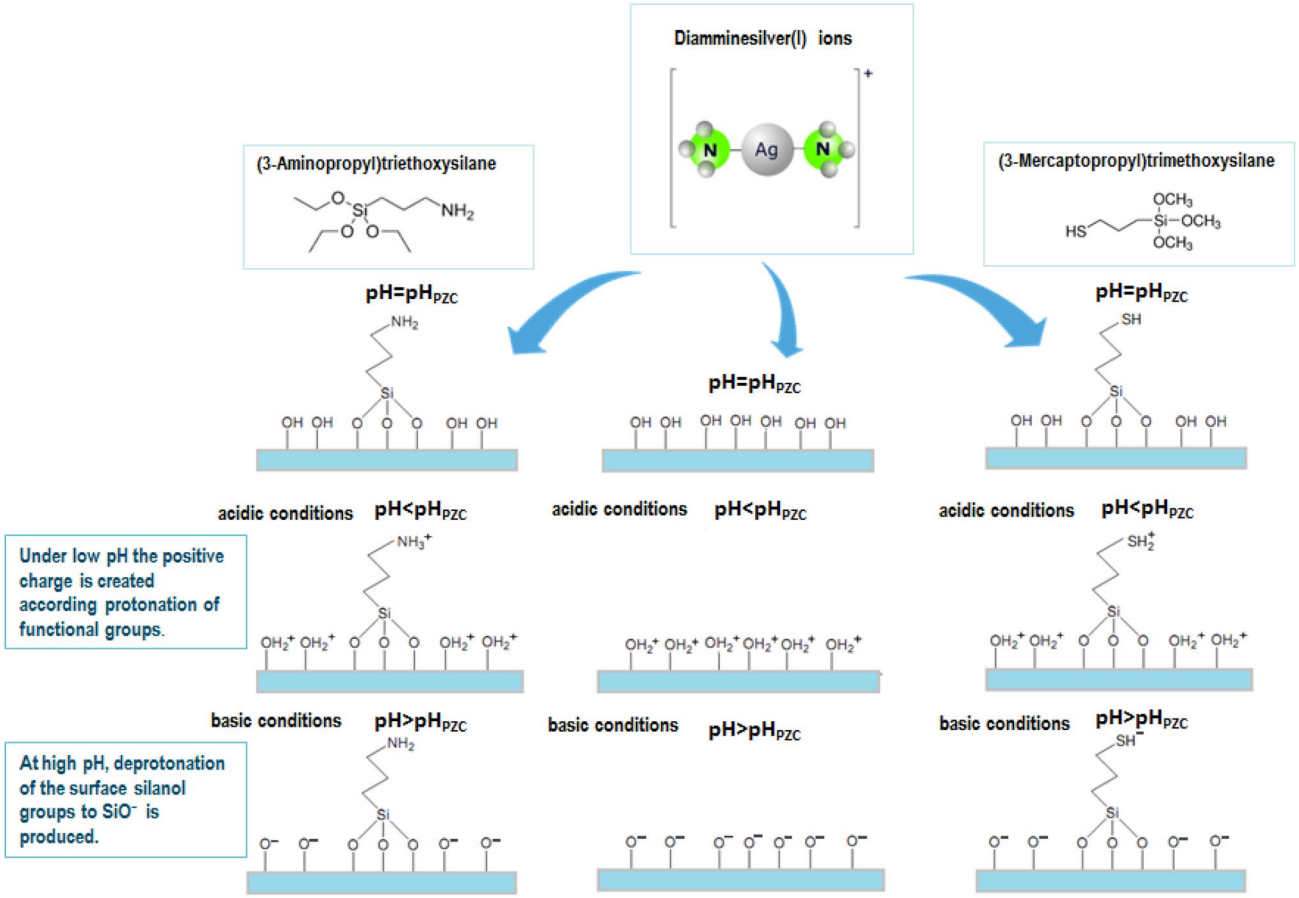

Fig. 3 Changing of the form of functional groups on APTES and MPTMS-functionalized silica surface after exposure to basic and acidic conditions

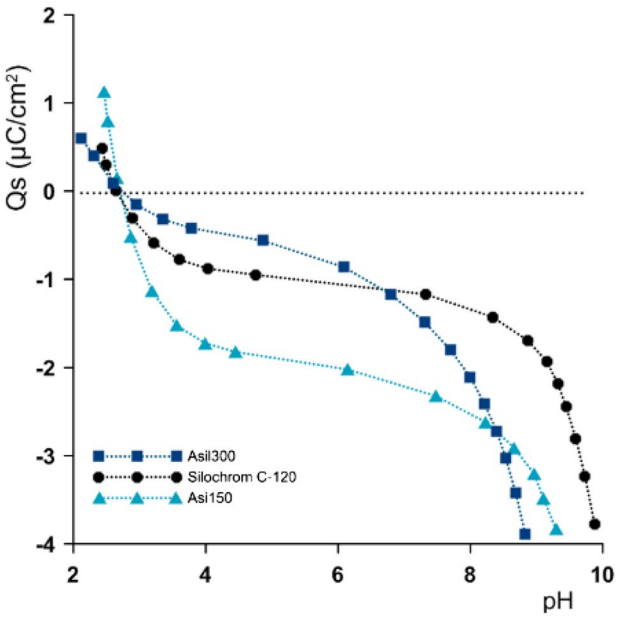

Fig. 4 Comparison of the surface charge density versus pH for pristine silica samples

by β_{ST} which is the instrument profile width (in this case 0.2): $\beta = \sqrt{\beta^2 - \beta ST^2}$.

All parameters should be calculated in radians.

The estimation the half-width for the last diffraction peaks can be quite difficult due to the low intensity and significant widening of the diffraction profile. For the most accurate analysis of the crystallite size, the special software for deconvolution of crystalline diffraction peaks from amorphous lines was applied (Rabiej 2014) (Fig. 6d). The results of the crystallite size analysis are present in Table 1. The general trend in changes of the size of silver crystallites taking into account the XRD analysis suggests that for silica samples without surface grafted with functional groups the size of silver crystallites is significantly lower than for the functionalized samples. Moreover, in the case of Silochrom sample, the silver nanoparticles have a very similar size with respect to the all visible crystal planes. The particles have size about 52, 52 and 57 nm as estimated for three crystallographic directions [(111), (200) and (220)], respectively. This can be evidence of the presence of small nanoparticles with the spherical shape. In the case of other Ag/silica

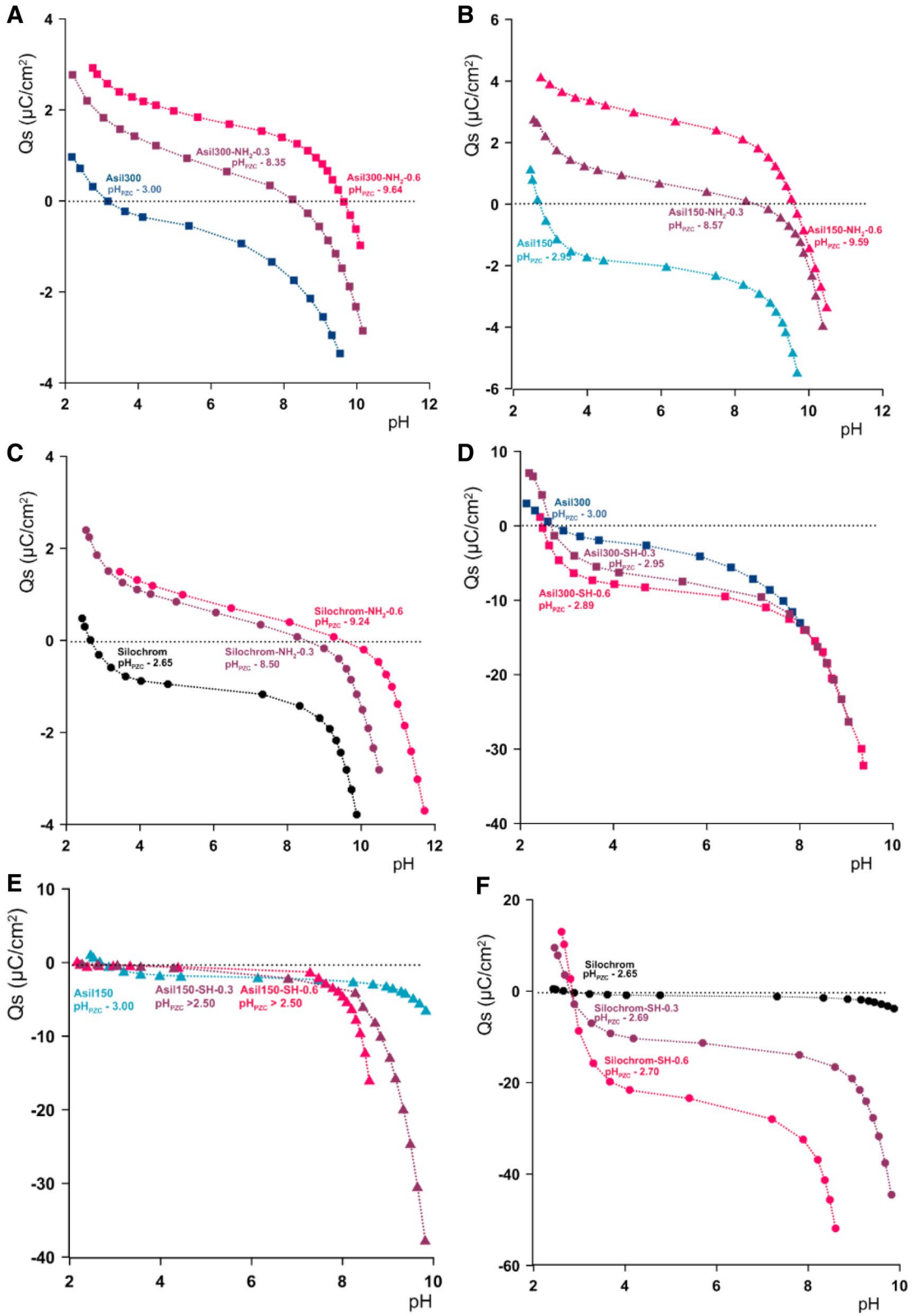

Fig. 5 pH dependence of surface charge density of silica samples functionalized by APTES and MPTMS

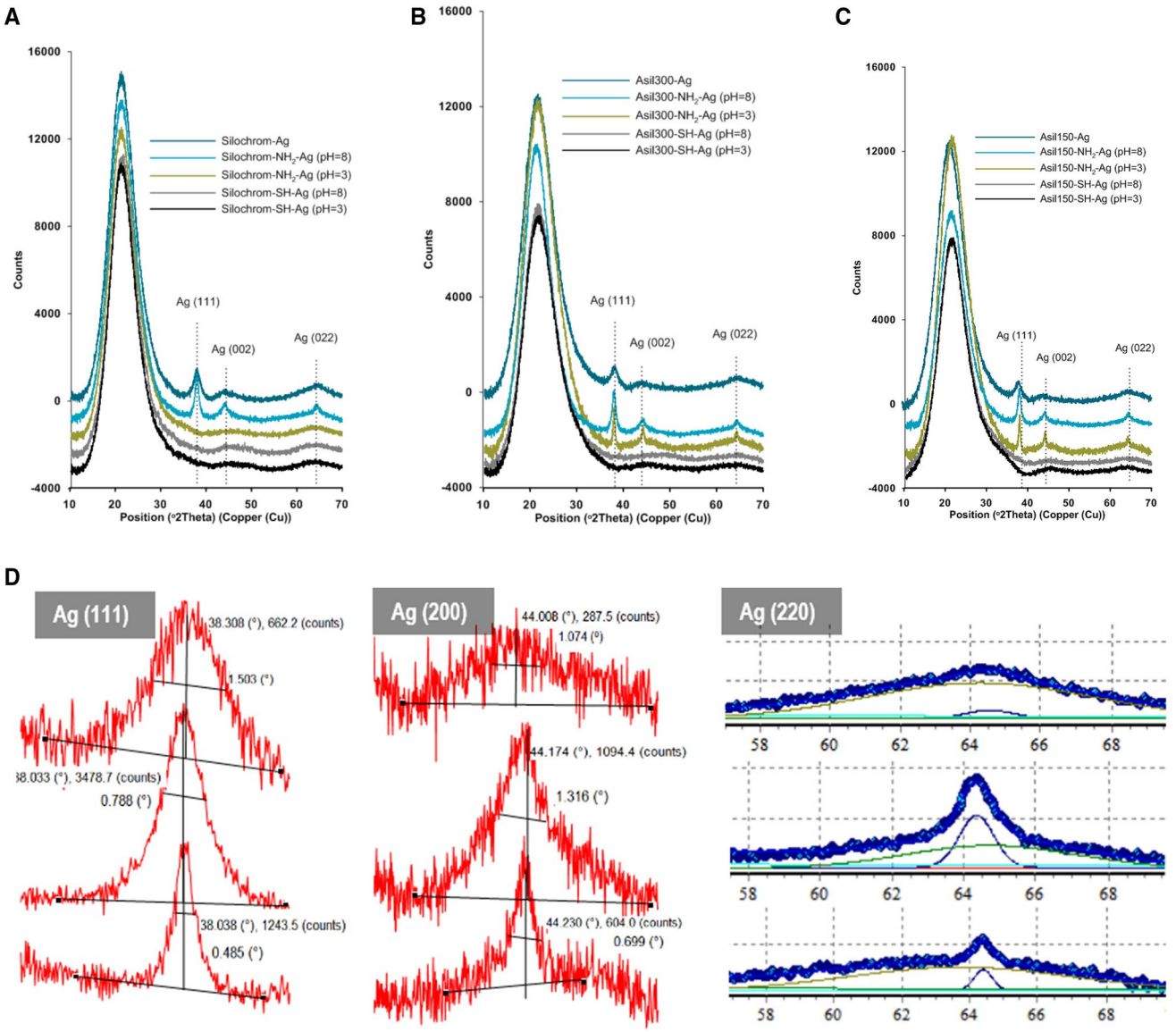

Fig. 6 Experimental XRD patterns for pyrogenic silica samples modified by functional groups and silver nanostructures: **a** Silochrom, **b** Asil 300 and **c** Asil 150, modified by functional groups and silver nanostructures on their surface. **d** Details of the observed diffraction patterns for Asil300-Ag as example. Experimental points, peak parameters and fitted profiles

composites (Asil300-Ag and Asil 150-Ag) without surface functionalization, the nanosilver creates also visible smaller forms, but the symmetry is not as good as for Silochrom. The average Ag particle size for Asil300-Ag sample was estimated to be about 5.6, 4.0 nm and below 2 nm from the peak width of Ag(111), Ag(200) and Ag(220), respectively.

Similar results were obtained for Asil150-Ag composite. In all cases using the amine-functionalized surface results in greater sizes of the particles obtained. When the conditions of impregnation were maintained at/near pH 8, the average size of obtained nanocrystalline silver is ~9, 11 and 10 nm as estimated from the width of Ag(111) for Silochrom-, Asil300- and Asil150-amine functionalized materials, respectively. Unfortunately, in the case of samples modified by thiol group, the crystal phase of silver was not observed, despite the same conditions and amount of silver precursor. In this case, silver nanoparticles, if present, are very small, below 2 nm.

Imaging the silver nanoparticles morphology: tapping mode of atomic force microscopy analysis and transmission electron microscopy

In this work, atomic force microscopy was used as a tool for imaging the silver nanostructures supported on pyrogenic silica careers both in the form of individual particles as well

Table 1 XPS and XRD parameters of investigated samples

Sample	% content Ag XPS	Ag crystal size (Å) in respect to the crystal planes		
		111	200	220
Silochrom-Ag (pH 8)	0.91	**52**	**52**	**57**
Silochrom-NH_2-Ag (pH 8)	0.97	90	44	66
Silochrom-NH_2-Ag (pH 3)	0.54	–	–	–
Asil300-Ag (pH 8)	1.81	**56**	**40**	**> 20**
Asil300-NH_2-Ag (pH 8)	2.30	107	66	55
Asil300-NH_2-Ag (pH 3)	0.71	187	124	122
Asil300-SH-Ag (pH 8)	0.66	–	–	–
Asil300-SH-Ag (pH 3)	0.21	–	–	–
Asil150-Ag (pH 8)	1.56	**58**	**40**	**> 20**
Asil150-NH_2-Ag (pH 8)	1.76	103	61	72
Asil150-NH_2-Ag (pH 3)	0.98	178	118	108

Bold values emphasize the smallest dimension of silver crystallites

as groups of particles and agglomerates. Moreover, the AFM imaging was applied to examine the effect related to properties of functionalized silica surface on the formation of the silver nanostructures. Here, the tapping mode of AFM was investigated for silver nanoparticle sizing purposes and their visualization in three dimensions. Tapping mode of AFM operation involves the cantilever position very close to the investigated surface and allows to map the topography of the sample by lightly tapping the surface with an oscillating probe tip. In effect, the lateral forces are reduced significantly which facilitates high-resolution imaging of soft and fragile samples in ambient conditions without inducing irreversible damage and image distortion. On the basis of this technique first, the differences between the materials before and after modification by silver nanostructures were illustrated. Figure 7 shows a comparison of AFM images of pure pyrogenic silica sample (Fig. 7a) and Ag/silica composite (Fig. 7b). Topography maps recorded for this case revealed the relatively smooth surface morphology of pyrogenic silica (an example of Asil300) with minimal irregularities in the form of valleys in the AFM images. It is clear that the surface of pure pyrogenic silica cannot be completely flat and uniform as a given case. The curvature of the surface is related to the presence of small pores which were usually located in valleys and confirmed and described in details as pore size distribution curves calculated from the nitrogen sorption isotherm. The surface modified by silver nanoparticles (Fig. 7b) has significantly more irregularities, deeper valleys, and distinguishable peaks, what suggests the formation of nearly spherical, round-shaped compounds with an average size of about below 50 nm. The surface coating by silver nanoparticles is fairly uniform with a high density of the deposited nanoparticles. Figure 7c, d present the line section of the AFM image displaying the height of features, so the size distribution of the silver nanoparticles was carried out by considering height profiles along the line marked in these data. Results clearly indicate that taking into account the sample height, the main part of the Ag nanoparticles for Asil300-NH_2-Ag (pH 8) sample were embedded in the range of 20–50 nm. In the case of the initial sample without silver nanostructures, the height of the heterogeneity elements visible on the amorphous silica surface falls within the range of 100–200 nm. In both cases, the valleys are significant (~ 200 nm) and still visible after silver nanoparticles deposition. In this work, we observed, that the size, morphology as well as the population of the silver nanoparticles distributed on silica surface depend on the pH conditions during silver ions deposition. The authors of this work agree that the size and shape of nanoparticles may be conditioned by many factors. In this part, the impact of pH on the size and morphology of the silver nanoparticles is considered as a result of changing the properties of surface functional groups. We observed that the size and distribution of the nanoparticle population are differentiated depending on pH applied during deposition. The observations and description of the sizes and shapes by AFM and XRD analysis have been confronted with TEM and SEM imaging (Fig. 7e–h). Some differences were observed between TEM and AFM images in terms of the size of silver nanoparticles. The AFM images suggest slightly larger sizes of silver nanoparticles compared with TEM, SEM, and XRD, while electron microscopies and X-ray diffraction results are very similar (particle diameters ~ 10 nm and lower). However, the AFM images provide three-dimensional surface profiles (information about the height of the sample) without any special treatments and interference in the sample. Taking into account certain restrictions of scanning probe microscopies (thermal drift on the sample during a long time of imaging, tip-sample forces and tip parameters) (Ruozi et al. 2014), electron microscopies and AFM techniques used simultaneously supply different and complementary data for investigation of nanomaterials.

It was observed that the mean particle size increased to form more aggregated phase with well-singled islands when pH decreased to ~ 3 (Fig. 8). Individual objects are still visible, but they form clearly defined clusters. It was also observed that in such conditions the resulting crystallites often feature an elongated shape (Fig. 9c).

At higher pH (pH ~ 8) the formation of silver nanoparticles with significantly smaller size and more homogeneous distribution on the silica surface was observed. The small objects are better separate and the space between them is more clearly outlined. Moreover, the shape of silver nanoparticles is more spherical what suggest obtaining the silver crystallites with higher symmetry. It is notable that the results of the pH influence on nanoparticles signalized in

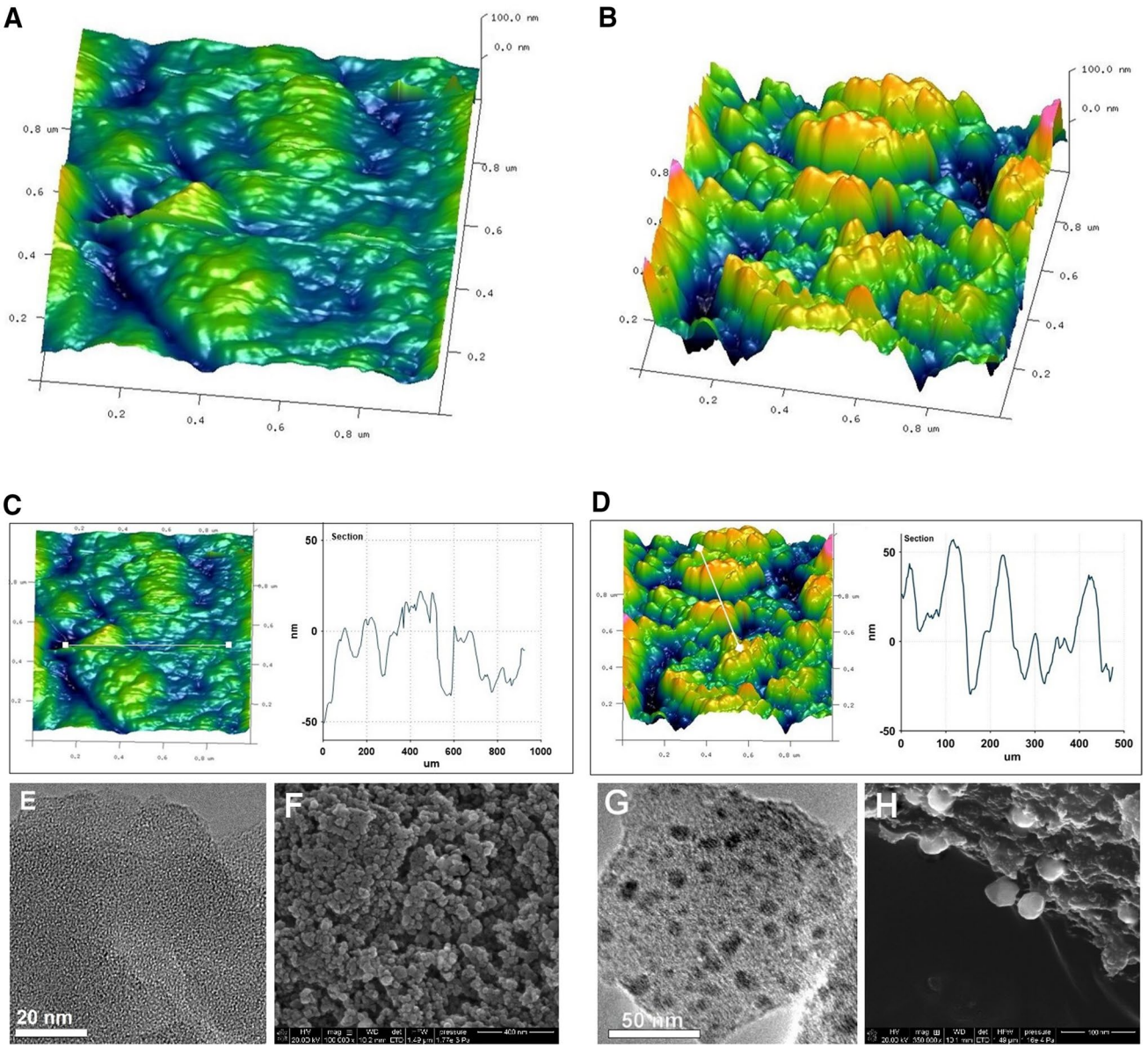

Fig. 7 **a** AFM 3D images (1 × 1 μm) representing the topography of pure Asil300, **b** AFM images (1 × 1 μm) representing the topography of Asil300 modified by NH_2 groups and silver nanoparticles (pH 8), **c** line profile of surface features along white line marked in 3D image for Asil300, **d** line profile of surface features along white line marked in 3D image for Asil300-NH_2-Ag (pH 8), **e** TEM and **f** SEM images of the pure Asil300 and **g** TEM and **h** SEM images of the Asil300-NH_2-Ag (pH 8) composites

this work are in good agreement with the results obtained in the literature (Alqadi et al. 2014).

The particle analysis from AFM data was performed to detect and measure the lateral and vertical dimensions of particles supported on the pyrogenic silica surfaces for samples prepared at pH 8 and pH 3. As a result, the diameter and height histograms of a topographical image were obtained to illustrate the statistical distribution of heights and diameters within the image. Both, diameter and high histogram for the sample obtained at lower pH confirms the greater size of deposited nanoparticles.

AFM imaging of the Asil300-SH-Ag (pH 8) indicates the presence of very small objects on the pyrogenic silica surface. The size of inhomogeneities does not exceed several nanometers, and it is difficult to define the real metallic nanoparticles in this case. The presence of very small objects was confirmed by TEM (Fig. 10d).

The principal question is what is the possible mechanism responsible for the formation of the small silver particles at high (pH ~ 8) and the large agglomerated population at low pH (~ 3) from $[AgNH_3]_2^+$. The role of the concentration of silver ions and a reducing agent is omitted in this case due

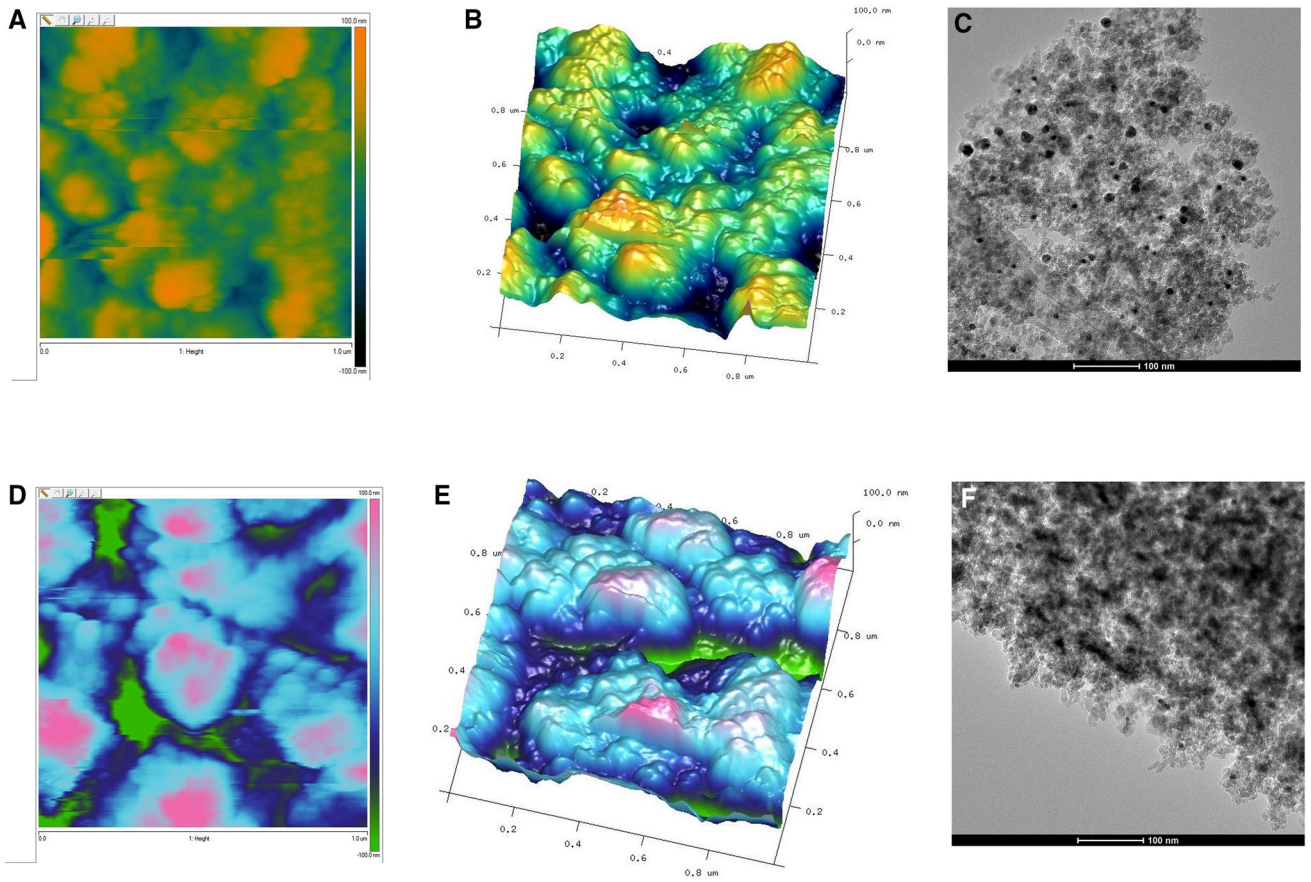

Fig. 8 AFM topography of the Asil150-NH_2-Ag illustrating pH effect on silver nanoparticles formation. **a** 2D and **b** 3D images (1 × 1 μm) for Asil150-NH_2-Ag sample prepared at pH 8, **c** TEM image of Asil150-NH_2-Ag (pH 8), **d** 2D topographic image and **e** 3D images of the same sample prepared at pH 3, **f** TEM image of Asil150-NH_2-Ag (pH 3)

to the same amount of silver precursor and thermal reduction procedure. One explanation of such difference in the size and form of silver nanoparticles depending on pH value can be attributed to their stability and various reduction rate of the silver precursor in solution. At high pH reduction rate is higher than at acidic condition due to the presence of OH^- ions. Moreover, taking into account only the effect of OH^- ions from solution on the formation of silver nanoparticles, it should be noted that in the presence of OH^- ions, the Ag^+ ions can adsorb on the particles surface with forming an electrical double layer as a protective layer of colloids. In this case, the effect of the agglomeration is reduced by an additional stabilization effect. At low pH oxidation effects may occur instead of the reduction of ions to the metallic state. In this work, except the various ions in solution phase, we have a functionalized surface with various properties at different pH. At low pH, the protonated $–NH_3^+$ group and $–OH_2^+$ groups are the source of the positive charge on the surface (Fig. 8). In this case, the repulsive electrostatic interactions between positively charged ions may be responsible for lowering stability of the system by lack or limitation of the interaction with the modified silica surface. In consequence, the greater silver crystallites with a tendency to agglomerate are observed. When the functional groups on silica surface possess a negative charge (–O–) at $pH > pH_{PZC}$ the additional stability of silver ions by surface may occur. Our observations allow concluding that the stabilization process conditioned by functional groups on silica surface applies both types of functional groups on the functionalized surface. The interpretation of such potential interaction was carried out by XPS analysis and presented in the following section of this work.

Electron spectroscopy for chemical analysis of silica/AgNP composites

The chemical state analysis of the investigated silica-silver nanocomposites was performed using X-ray photoelectron spectroscopy. Thus, photoelectron spectra were obtained to analyze the chemical state of elements forming the nanocomposite structure and to get information of the surface layers of materials. In particular, the qualitative analysis, as well

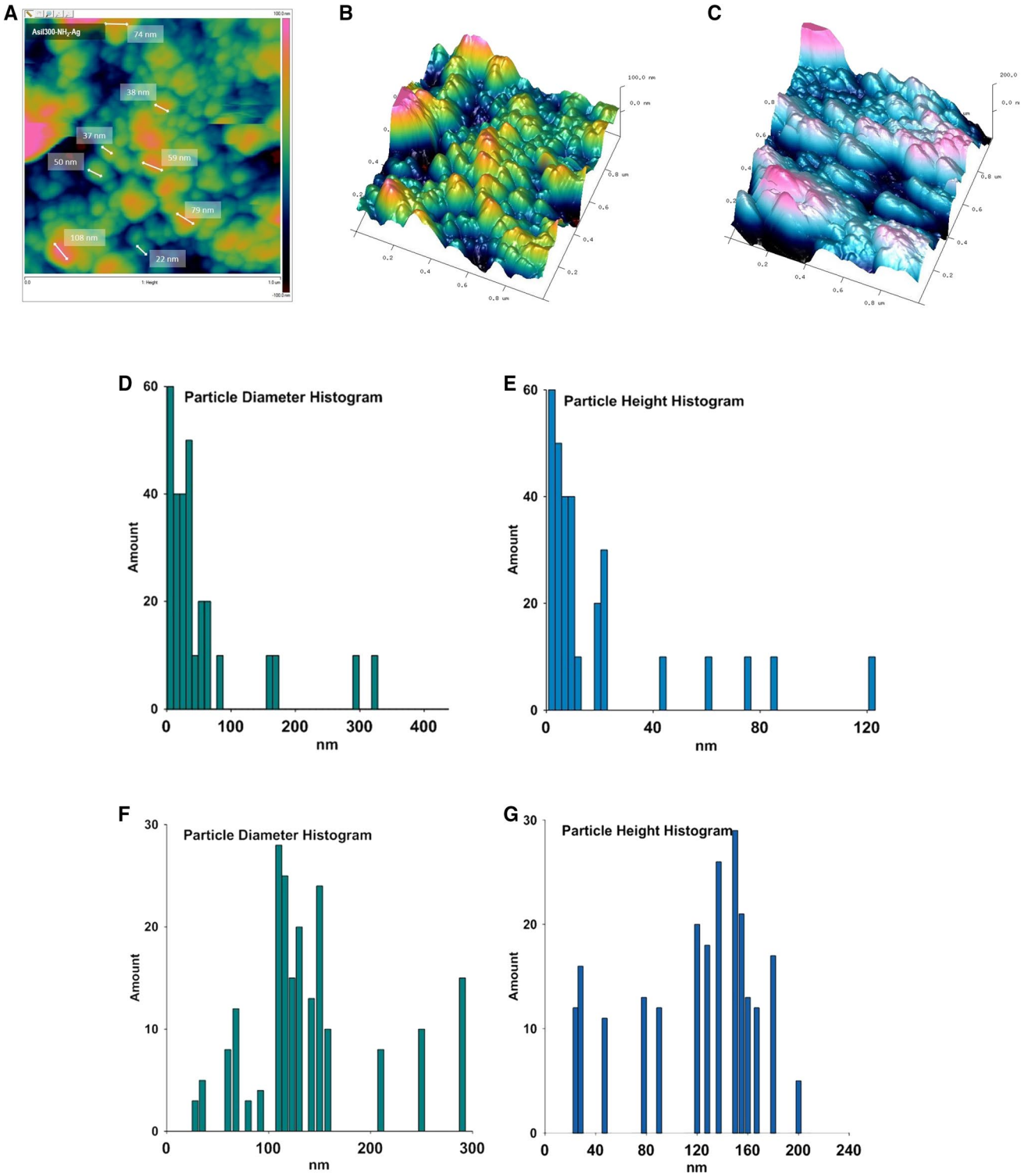

Fig. 9 Particle analysis from AFM images. **a** AFM 2D topographic image of Asil300-NH_2-Ag sample with cross-section of silver objects, **b** 3D AFM image of sample prepared at pH 8, **c** the same sample prepared at pH 3. **d, e** Particle diameter and particle height distributions estimated from picture **b. f, g** Particle diameter and particle height distributions estimated from picture **c**

as the proportional content of the elements with the binding assignation was performed to describe the mechanism of adsorption of the silver ions. The obtained XPS results are presented in Table 2. The XPS survey spectra show the

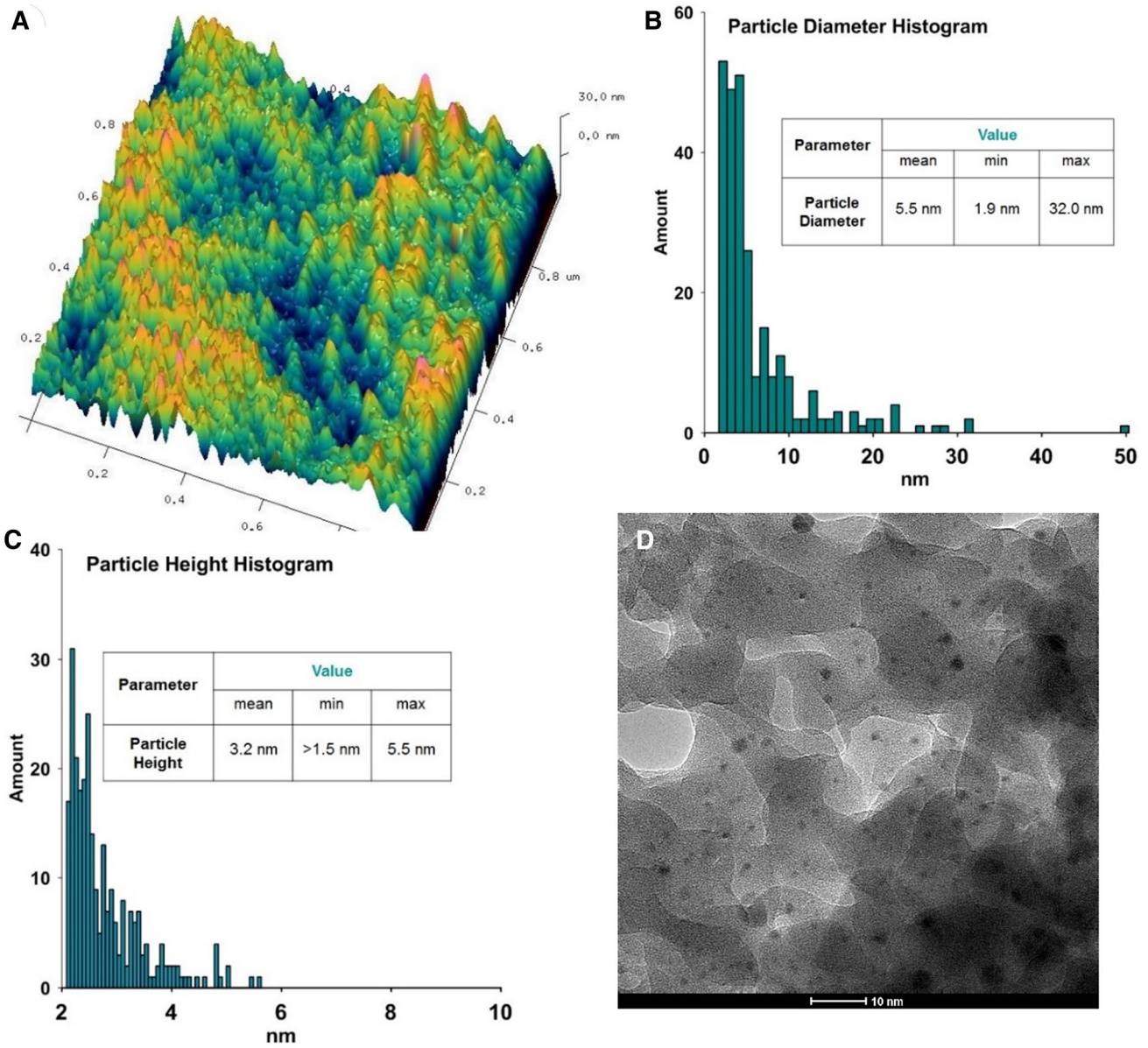

Fig. 10 Particle analysis from AFM images performed for Asil300-SH-Ag (pH 8) sample. **a** 3D AFM image, **b, c** particle diameter and particle height distributions estimated from picture **a. d** TEM image of as-prepared Asil300-SH-Ag (pH 8) sample

spectral lines of photoelectrons from elements in the binding energy scale of 0–1200 eV (Fig. 11a).

The major signals observed in XPS spectra for Asil300-NH_2-Ag (pH 8) were identified as O1s, Ag3d, Si2p as well as directly related O2s and Si2s signals. In the case of initial sample (Asil300-NH_2-06 without silver nanoparticles) the N1s signal was also identified. We failed to observe the N1s signal for Asil300-NH_2-Ag (pH 8) sample. One explanation for this phenomenon is based on obscuring effect of silane coupling agent by silver nanoparticles. In this case, the proportional content of carbon is also significantly lower and equals 0.4% instead of 9.7% determined for initial sample.

Calculating the amount of nitrogen which is attributable to the indicated carbon content (for 0.4% of carbon, proportional content of nitrogen is below 0.1%) and the assumption that all carbon is associated with the presence of (3-aminopropyl) triethoxysilane, the amount of nitrogen is too small to correctly designate their presence by XPS. The silver nanoparticles are created at the same place as silane coupling agent. The average depth of analysis for an XPS measurement is approximately several nm (most often 5 nm). If the dimensions of particles are larger than the depth of analysis

Table 2 XPS results for Asil300-NH_2 (amount of NH_2 groups 0.6 mmol/g) and Asil300-NH_2-Ag (pH 8) samples

Sample	Name	Peaks position (eV)	Full width at half maximum (FWHM)	Atomic concentration (%)	% st. dev.		Mass concentration (%)
Asil300-NH_2-06	C 1s	285.5	3.03	12.5	0.2	9.7	
	O 1s	533.0	2.43	48.6	0.2	38.5	
	Si 2p	103.5	2.52	36.3	0.2	50.3	
	N 1s	401.0	3.32	2.6	0.1	1.5	
Asil300-NH_2-Ag (pH 8)	C 1s	285.0	1.83	0.7	0.2	0.4	
	O 1s	532.0	2.52	56.4	0.2	44.3	
	Si 2p	103.5	2.65	40.3	0.1	53	
	Ag 3d	367.3	2.12	2.6	0.1	2.3	
					Area		Binding assignation
	O 1sB	532.7	1.95	96.0	51,073		SiO_2
	O 1sA	529.5	1.89	4.0	2011		Ag_2O
	Si 2p	103.5	1.98	100.0	9785		SiO_2
	Ag 3d 5/2 C	367.7	1.40	23.0	106		Ag (I) Ag_2O, Ag (II) AgO
	Ag 3d 5/2 B	368.3	1.74	50.0	237		Ag (0)
	Ag 3d 5/2 A	369.3	2.00	27.0	130		Ag–N
	Ag 3d 3/2 C	373.7	1.40	–	71		
	Ag 3d 3/2 B	374.3	1.45	–	158		
	Ag 3d 3/2 A	375.3	1.80	–	87		

Positions of general peaks as a signal of photoelectrons from various energetic levels and high-resolution analysis and their assignment

the underneath functional groups are not visible. A similar effect was observed by other researchers, but no explanation has been offered (Huang et al. 2015).

The proportional content of silver in Asil300-NH_2-Ag (pH 8) was greater than the proportional content of nitrogen in the initial sample. This may confirm that oxygen species on silica surface may interact with silver ions/silver nanoparticles beside amino groups from (3-aminopropyl) triethoxysilane. The proportional content of silver for other samples is presented in Table 1. A general tendency was observed in the enhancement of silver content for materials obtained at pH 8 and samples modified by ammine groups. In all cases, the proportional content of silver was slightly lower when the surface was not further modified and substantially lower when the conditions were determined as pH 3. Moreover, the significantly lower proportional content of silver was achieved for silica materials functionalized by thiol groups. However, the dependence of the amount of AgNP in a relation to the surface modification has been still maintained. Our observations indicate that for silica decorated by thiol groups the procedure of silver deposition at pH 8 allows for three times more effective modification of the silica material by AgNP than applying the pH ~ 3.

In this case, the interactions between the silver precursor and pyrogenic silica surface are of the greatest importance. Detailed XPS spectra, registered with a higher resolution permits analysis of chemical composition, chemical shifts and, therefore, the chemical state of observed chemical bonds and valences. To determine the oxidation state of silver atoms the measurement at the Ag3d core levels was carried out. The survey scan XPS spectra for Asil300-NH_2-Ag (pH 8) and Asil300-NH_2-06 as an example, as well as deconvolution of Ag3d spin–orbital splitting, is shown in Fig. 11. For samples modified by silver nanoparticles the Ag3d signal consist of peaks doublet for silver corresponding to 3/2 and 5/2 spin states (for $l=2$, $s=\pm 1/2$). The position of the silver doublet in the case of Asil300-NH_2-Ag (pH 8) (and very similar for other examples) appears at 367.3 and 373.3 eV for Ag3d5/2 and Ag3d3/2 peaks, respectively, and is lower about 1 eV than binding energy characteristic for silver in the metallic state (Battocchio et al. 2012; Wang et al. 2012; NIST 2012). The splitting of the Ag 3d doublet (the differences between Ag3d5/2 and Ag3d3/2 signals) is properly marked as 6 eV (Ferraria et al. 2012). Figure 11b shows three spin–orbit pairs of XPS signals for Ag3d5/2 and Ag3d3/2 energetic levels as a fitting of experimental curve. The main signals within Ag 3d peaks are located at 368.3 and 374.3 eV for Ag3d5/2B and Ag3d3/2B components and can be identified as metallic silver atoms in the bulk phase of silver nanoparticles (Kaushik 1991; Hoflund et al. 2000; Bao et al. 1996; Moulder et al. 1992). The binding energy for another spin–orbit pair shifts towards lower binding energy values at the positions 367.7 and 373.7 eV for Ag3d5/2C and Ag3d3/2C lines, respectively, are attributed to the silver atoms bonding with oxygen suggesting the existence of silver(I) and silver(II) oxidation states in Ag_2O (Weaver and

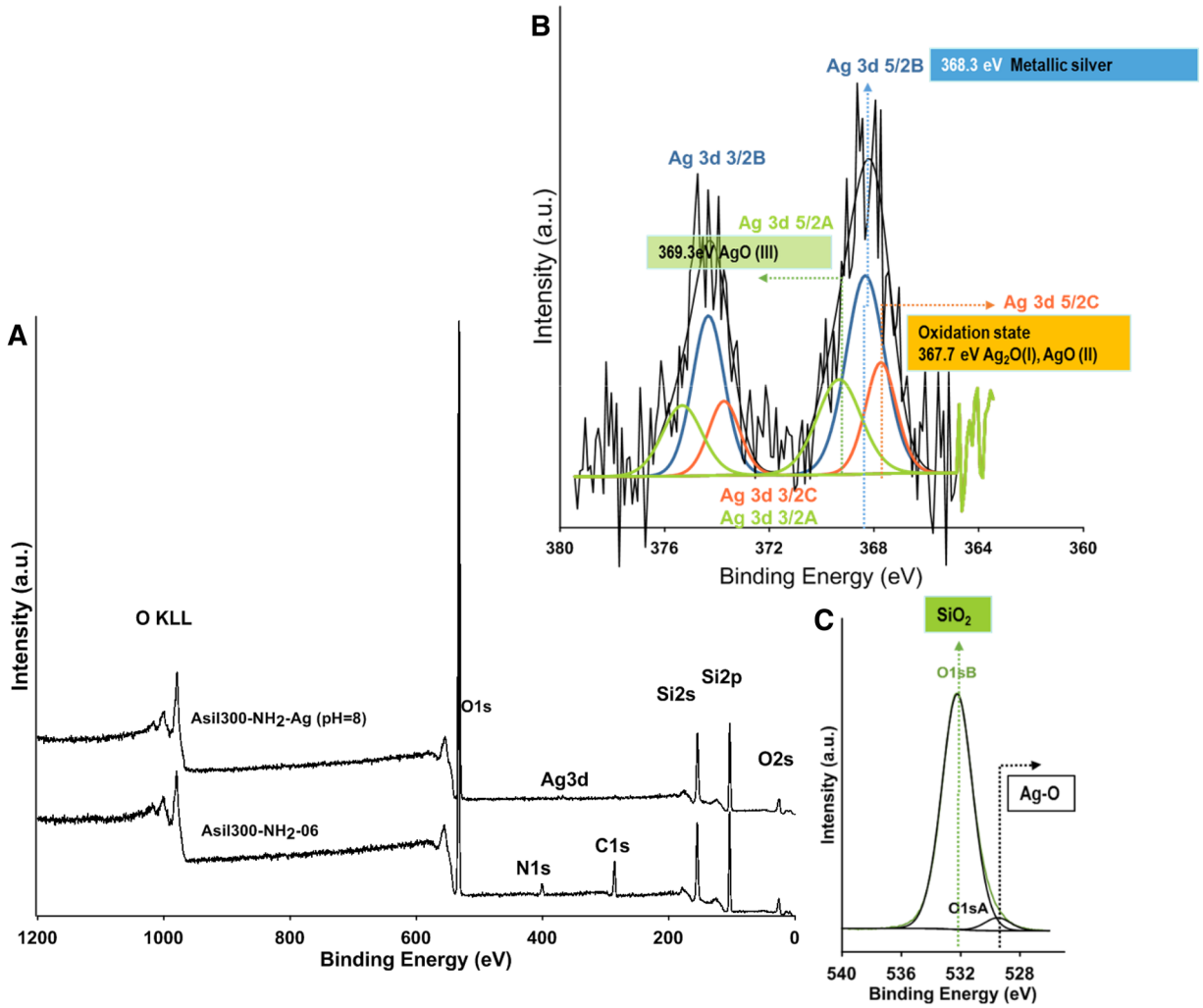

Fig. 11 XPS spectra of pyrogenic silica modified by amine groups and silver nanoparticles

Hoflund 1994) and AgO phase (Schon 1973) (confirmed also for oxygen atoms in Fig. 11c). The third spin–orbit pair at position 369.3 and 375.3 eV for Ag3d5/2A and Ag3d3/2A, respectively, is shifted about 1 eV from position characteristic to metallic silver phase and can be attributed with the higher oxidation state of silver (Battocchio et al. 2012). The binding energy for Ag3d5/2A and Ag3d3/2A lines is related to interaction with amino groups and in the case of Asil300-SH-Ag (pH 8) also with thiol groups. The interpretation of interactions between silver and nitrogen or sulfur atoms was based on the similar observations in the shift of binding energy to higher values for Ag3d lines based on researchers in the actual literature (Nivethaa et al. 2015). Interesting explanation describe the role of Ag particles as donates of electrons and generate the shift of binding energy to higher value (Ren et al. 2015) The presence of silver–nitrogen interaction indicates that apart from interactions between silver ions and oxygen atoms from hydroxyl groups (i.e., groups with different charges at pH 8), the interactions between the amino groups and the silver ions are also important. In the case of the thiol-modified sample, the proportional content of silver is significantly smaller and equals about 0.66% what causes that Ag3d signals are weaker and not so good marked as in the case of Asil300-NH_2-Ag (pH 8) sample. Still, the shift of binding energy to near 369 eV can be observed and suggests the bonding of silver atoms with thiol groups through the S-bridge (Ag). The possible mechanism of the formation of ultra-small silver nanoparticles with commitment of thiol can be based on the faster reduction of silver precursor by more electron rich thiol groups. As a result the Ag-S-R clusters are formed on the surface rather than well-defined crystal structures. This effect can be confirmed by lack of the crystal structures visible by XRD and the existence of the binding energy shift by XPS. Based on the detailed analysis, it was found that about 50% of silver is in the Ag^0 chemical state, while about 23% were in Ag^+

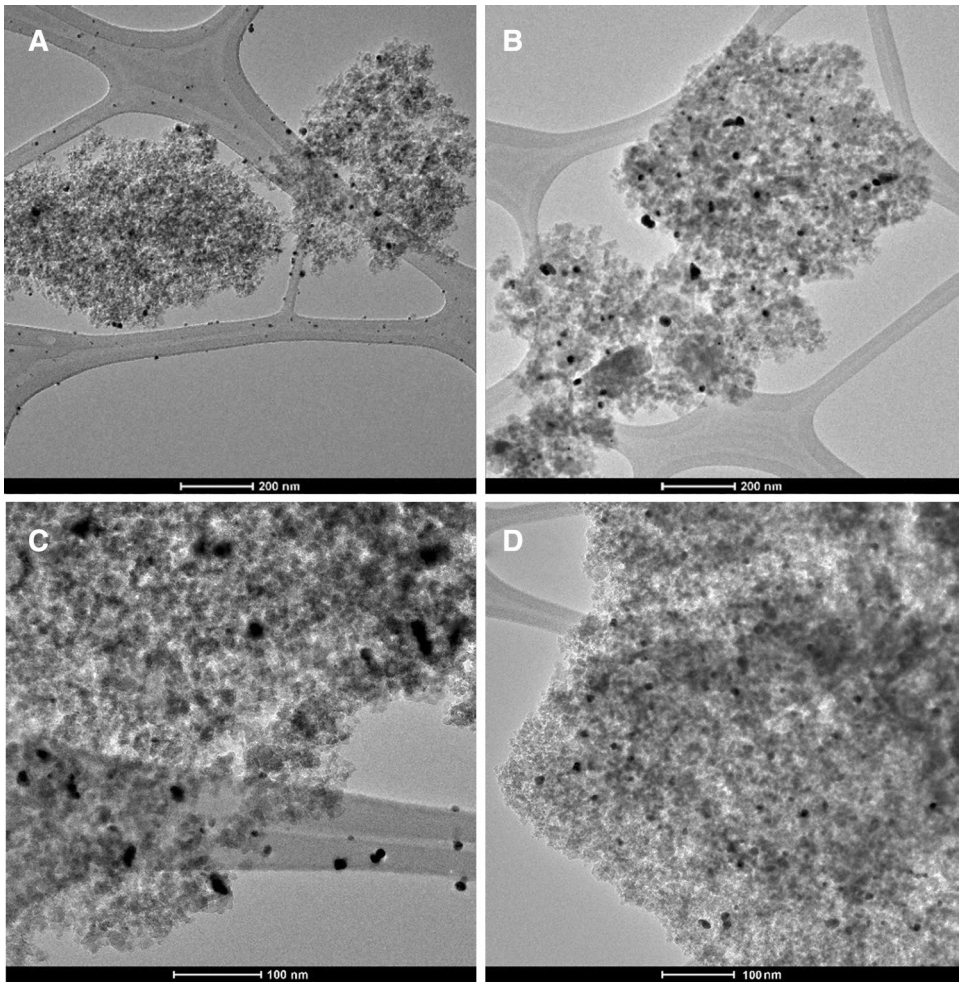

Fig. 12 TEM images of **a, c** Asil300-NH_2-Ag (pH 3) and **b, d** Asil300-NH_2-Ag (pH 8) samples

and Ag^{2+} chemical states and quite significant 27% in more oxidized silver states, respectively. The shift of binding energy to lower values for silver oxides is different than the expected shift and electronegativity rules (typical connection with more electronegative components causes the increasing of binding energy). In the case of silver compounds, many other factors based on lattice energy and extra-atomic relaxation energies are influenced on final shift of binding energy and discussed in details in the literature (Gaarenstroom and Winograd 1977; Wolan and Hoflund 1998).

Moreover, the lower amount of silver nanoparticles on the silica surface when acidic conditions were applied may be related to the significantly lower interaction of metal nanoparticles with the surface. The clear evidence of this phenomena was found after TEM consideration. Figure 12 shows the TEM images of two samples: Asil300-NH_2-Ag (pH 3) and Asil300-NH_2-Ag (pH 8). It was observed the clear migration of the nanoparticles from the surface of silica to carbon membrane of TEM grid (Fig. 12a).

This means no chemical interaction with the silica surface, low stability of the nanoparticles on this surface and the ability to transport them to a surface with higher affinity when the acidic conditions during their deposition are used. Figure 12b shows different situation for basic conditions. Silver nanoparticles remained stably bound to the surface of the silica phase. TEM images at higher magnification and collected from other area of sample (for comparison) (Fig. 12c, d for pH 3 and pH 8 respectively) illustrate a better degree of distribution the nanoparticles on the surface. The silver nanophase at pH 8 remain smaller and do not escape beyond the surface of the carrier.

Conclusions

The description of the surface chemistry of nanomaterials and their behavior in respect to other substances and biomolecules is a very challenging problem. In particular, in the case of silver nanoparticles-based nanocomposites, the assessment of surface chemistry seems to be important and worth more detailed description. In this work, we have studied the effect of the size, shape, and distribution of the silver nanoparticles depending on the chemical state of the functionalized solid support. Also worthy of note is

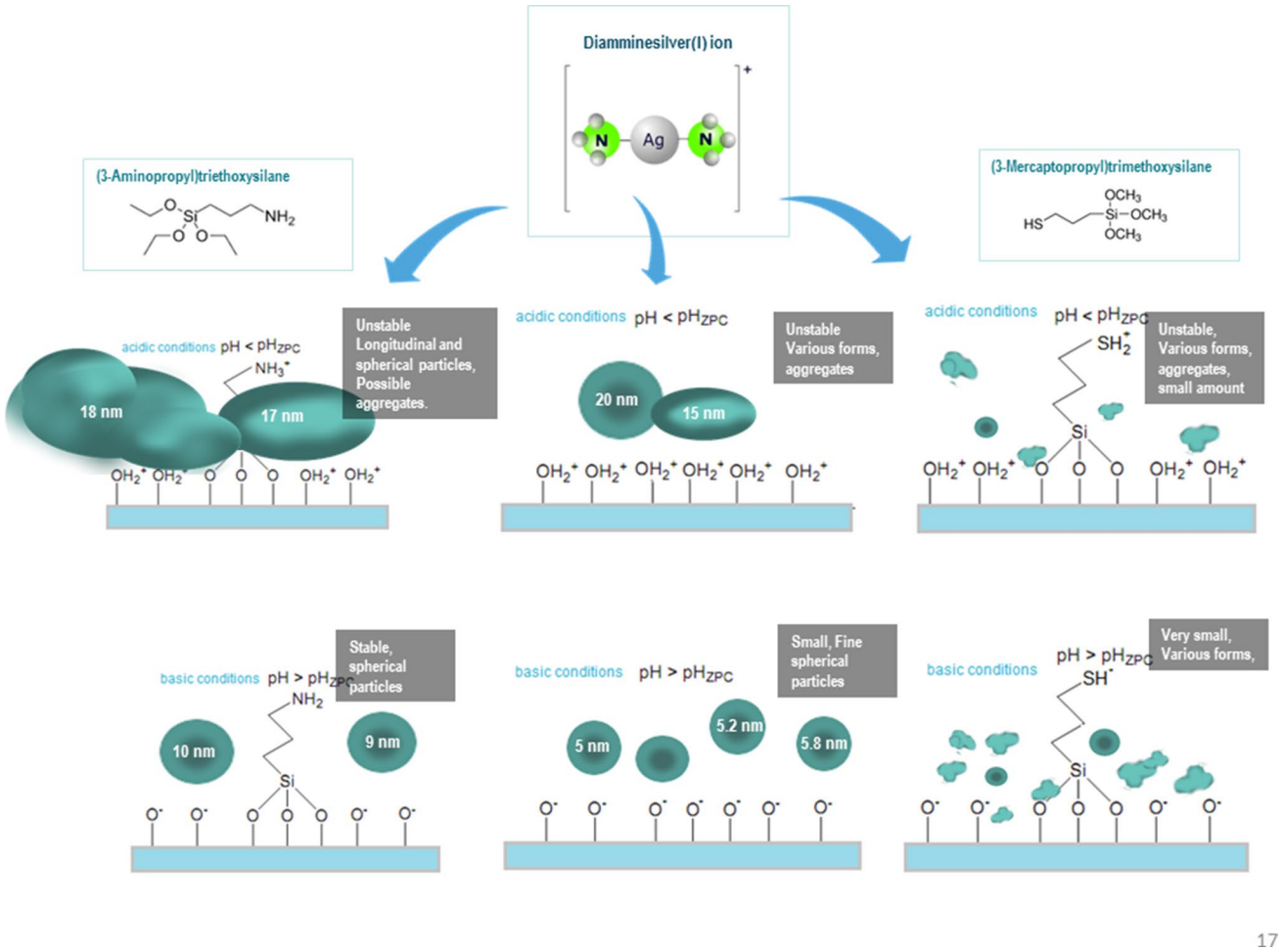

Fig. 13 Summary of the obtained results. Size and morphology of the AgNP depending on surface properties

the comprehensive approach to addressing the challenges of impact of pH conditions on the properties of silver nanoparticles. The PZC is the very important parameter which plays a crucial role in various chemical phenomena with multi-application potential. Atomic-force microscope (AFM) and XRD analysis were applied to describe the silver crystallite size and shape and illustrate the three-dimensional images of a surface of Ag/silica solid state with nanoscale resolution. The results show the influence of silver nanostructures doping on the topography of the pyrogenic silica and the observed differences can be associated with changes in processing conditions and the support surface due to various conditions. The possible interactions between components were investigated in detail by XPS. The summary can be easily illustrated in Fig. 13. The results of our investigations allowed to apply the nanocomposites of various degree of aggregation (various size and shape of metal nanoparticles) in the Raman spectroscopy measurements to increase the Raman signal in the case of samples with low spectroscopic response.

Acknowledgements The research leading to these results has received funding from the People Programme (Marie Curie Actions) of the European Union's Seventh Framework Programme FP7/2007-2013/ under REA Grant Agreement no. PIRSES-GA-2013-612484.

References

Alqadi MK, Noqtah OAA, Alzoubi FY, Alzouby J, Aljarrah K (2014) pH effect on the aggregation of silver nanoparticles synthesized by chemical reduction. Mater Sci Pol 32:107–111. https://doi.org/10.2478/s13536-013-0166-9

Ashtari P, He XX, Wang KM, Gong P (2005) An efficient method for recovery of target ssDNA based on amino-modified silica-coated

magnetic nanoparticles. Talanta 67:548–554. https://doi.org/10.1016/j.talanta.2005.06.043
Balagna C, Perero S, Ferraris S, Miola M, Fucale G, Manfredotti C et al (2012) Antibacterial coating on polymer for space application. Mater Chem Phys 135:714–722. https://doi.org/10.1016/j.matchemphys.2012.05.049
Bao X, Muhler M, SchedelNiedrig T, Schlogl R (1996) Interaction of oxygen with silver at high temperature and atmospheric pressure: a spectroscopic and structural analysis of a strongly bound surface species. Phys Rev B 54:2249–2262. https://doi.org/10.1103/PhysRevB.54.2249
Battocchio C, Meneghini C, Fratoddi I, Venditti I, Russo MV, Aquilanti G, Maurizio C, Bondino F, Matassa R, Rossi M, Mobilio S, Polzonetti G (2012) Silver nanoparticles stabilized with thiols: a close look at the local chemistry and chemical structure. J Phys Chem C 116:19571–19578. https://doi.org/10.1021/jp305748a
Bindhu MR, Umadevi M (2014) Silver and gold nanoparticles for sensor and antibacterial applications. Spectrochim Acta Part A Mol Biomol Spectrosc 128:37–45. https://doi.org/10.1016/j.saa.2014.02.119
Broekhoff JCP (1979) Mesopore determination from nitrogen sorption isotherms: fundamentals, scope, limitations. Stud Surf Sci Catal 3:663–684. https://doi.org/10.1016/S0167-2991(09)60243-3
Brown J, Richer R, Mercier L (2000) One-step synthesis of high capacity mesoporous Hg^{2+} adsorbents by non-ionic surfactant assembly. Microporous Mesoporous Mater 37:41–48. https://doi.org/10.1016/s1387-1811(99)00191-2
Cao G (2004) Nanostructures & nanomaterials: synthesis, properties & applications. World scientific publishing Co. Pte. Ltd./Imperial College Press, London
Chang KC, Lin CY, Lin HF (2008) Thermally and mechanically enhanced epoxy resin-silica hybrid materials containing primary amine-modified silica nanoparticles. J Appl Polym Sci 108:1629–1635. https://doi.org/10.1002/app.27559
Chen ZL, Hsu FC, Battigelli D, Chang HC (2006) Capture and release of viruses using amino-functionalized silica particles. Anal Chim Acta 569:76–82. https://doi.org/10.1016/j.aca.2006.03.103
Chimentao RJ, Kirm I, Medina F, Rodriguez X, Cesteros Y, Salagre P et al (2004) Different morphologies of silver nanoparticles as catalysts for the selective oxidation of styrene in the gas phase. Chem Commun 7:846–847. https://doi.org/10.1039/b400762j
Chiron N, Guilet R, Deydier E (2003) Adsorption of Cu(II) and Pb(II) onto a grafted silica: isotherms and kinetic models. Water Res 37:3079–3086. https://doi.org/10.1016/s0043-1354(03)00156-8
Cullity BD (1978) In elements of X-ray diffraction. Addison-Wesley, London, p 101
Curran JM, Chen R, Hunt JA (2005) Controlling the phenotype and function of mesenchymal stem cells in vitro by adhesion to silane-modified clean glass surfaces. Biomaterials 26:7057–7067. https://doi.org/10.1016/j.biomaterials.2005.05.008
Dharanivasan G, Rajamuthuramalingam T, Michael Immanuel Jesse D, Rajendiran N, Kathiravan K (2015) Gold nanoparticles assisted characterization of amine functionalized polystyrene multiwell plate and glass slide surfaces. Appl Nanosci 5:39–50. https://doi.org/10.1007/s13204-014-0311-8
Elechiguerra JL, Burt JL, Morones JR, Camacho-Bragado A, Gao X, Lara HH, Yacaman MJ (2005) Interaction of silver nanoparticles with HIV-1. J Nanobiotechnol 3:1–10. https://doi.org/10.1186/1477-3155-3-6
Farooq U, Tweheyo MT, Sjoblom J, Oye G (2011) Surface characterization of model, outcrop, and reservoir samples in low salinity aqueous solutions. J Dispers Sci Technol 32:519–531. https://doi.org/10.1080/01932691003756936
Ferraria AM, Carapeto AP, Botelho do Rego AM (2012) X-ray photoelectron spectroscopy: silver salts revisited. Vacuum 86:1988–1991. https://doi.org/10.1016/j.vacuum.2012.05.031
Ferraris S, Perero S, Verne E, Battistella E, Rimondini L, Ferraris M (2011) Surface functionalization of Ag-nanoclusters-silica composite films for biosensing. Mater Chem Phys 130:1307–1316. https://doi.org/10.1016/j.matchemphys.2011.09.019
Forest V, Cottier M, Pourchez J (2015) Electrostatic interactions favor the binding of positive nanoparticles on cells: a reductive theory. Nano Today 10:677–680. https://doi.org/10.1016/j.nantod.2015.07.002
Gaarenstroom SW, Winograd N (1977) Initial and final-state effects in esca spectra of cadmium and silver-oxides. J Chem Phys 67:3500–3506. https://doi.org/10.1063/1.435347
Galiano K, Pleifer C, Engelhardt K, Brossner G, Lackner P, Huck C et al (2008) Silver segregation and bacterial growth of intraventricular catheters impregnated with silver nanoparticles in cerebrospinal fluid drainages. Neurol Res 30:285–287. https://doi.org/10.1179/016164107x229902
Giri N,. Natarajan RK, Gunasekaran S, Shreemathi S (2011) Arch Appl Sci Res 3:624–630
Gittins DI, Caruso F (2002) Biological and physical applications of water-based metal nanoparticles synthesised in organic solution. ChemPhysChem 3:110–113. https://doi.org/10.1002/1439-7641(20020118)3:1%3C110::aid-cphc110%3E3.0.co;2-q.
Gojova A, Guo B, Kota RS, Rutledge JC, Kennedy IM, Barakat AI (2007) Induction of inflammation in vascular endothelial cells by metal oxide nanoparticles: effect of particle composition. Environ Health Perspect 115:403–409. https://doi.org/10.1289/ehp.8497
Haddada MB, Blanchard J, Casale S, Krafft JM, Vallee A, Methivier C, Boujday S (2013) Optimizing the immobilization of gold nanoparticles on functionalized silicon surfaces: amine- vs thiol-terminated silane. Gold Bull 46:335–341. https://doi.org/10.1007/s13404-013-0120-y
He BL, Tan JJ, Kong YL, Liu HF (2004) Synthesis of size controlled Ag nanoparticles. J Mol Catal A Chem 221(1–2):121–126. https://doi.org/10.1016/j.molcata.2004.06.025
He XX, Huo HL, Wang KM, Tan WH, Gong P, Ge J (2007) Plasmid DNA isolation using amino-silica coated magnetic nanoparticles (ASMNPs). Talanta 73:764–769. https://doi.org/10.1016/j.talanta.2007.04.056
Hiramatsu H. Osterloh FE (2004) A simple large-scale synthesis of nearly monodisperse gold and silver nanoparticles with adjustable sizes and with exchangeable surfactants. Chem Mater 16:2509–2511. https://doi.org/10.1021/cm049532v
Hoflund GB, Hazos ZF, Salaita GN (2000) Surface characterization study of Ag, AgO, and Ag_2O using X-ray photoelectron spectroscopy and electron energy-loss spectroscopy. Phys Rev B 62:11126–11133. https://doi.org/10.1103/PhysRevB.62.11126
Huang RS, Hou BF, Li HT, Fu XC, Xie CG (2015) Preparation of silver nanoparticles supported mesoporous silica microspheres with perpendicularly aligned mesopore channels and their antibacterial activities. RSC Adv 5:61184–61190. https://doi.org/10.1039/c5ra06358b
Ju-Nam Y, Lead JR (2008) Manufactured nanoparticles: an overview of their chemistry, interactions and potential environmental implications. Sci Total Environ 400:396–414. https://doi.org/10.1016/j.scitotenv.2008.06.042
Katz E, Willner I (2004) Integrated nanoparticle-biomolecule hybrid systems: synthesis, properties, and applications. Angew Chem Int Ed 43:6042–6108. https://doi.org/10.1002/anie.200400651
Kaushik VK (1991) XPS core level spectra and auger parameters for some silver compounds. J Electron Spectrosc Relat Phenom 56:273–277. https://doi.org/10.1016/0368-2048(91)85008-h
Kim J, Lee J, Kwon S, Jeong S (2009) Preparation of biodegradable polymer/silver nanoparticles composite and its antibacterial

efficacy. J Nanosci Nanotechnol 9:1098–1102. https://doi.org/10.1166/jnn.2009.C096
Kosmulski M (2002) The pH-dependent surface charging and the points of zero charge. J Colloid Interface Sci 253:77–87. https://doi.org/10.1006/jcis.2002.8490
Liu W, Howarth M, Greytak AB, Zheng Y, Nocera DG, Ting AY et al (2008) Compact biocompatible quantum dots functionalized for cellular imaging. J Am Chem Soc 130:1274–1284. https://doi.org/10.1021/ja076069p
Love JC, Estroff LA, Kriebel JK, Nuzzo RG, Whitesides GM (2005) Self-assembled monolayers of thiolates on metals as a form of nanotechnology. Chem Rev 105:1103–1169. https://doi.org/10.1021/cr0300789
Mercier L, Pinnavaia TJ (1998) A functionalized porous clay heterostructure for heavy metal ion (Hg^{2+}) trapping. Microporous Mesoporous Mater 20:101–106. https://doi.org/10.1016/s1387-1811(97)00019-x
Milczarek G, Motylenko M, Sikorska AM, Klapiszewski Ł, Wysokowski M, Bazhenov VV, Piasecki A, Konował E, Ehrlich H, Jesionowski T (2014) Deposition of silver nanoparticles on organically-modified silica in the presence of lignosulfonate. RSC Adv 4:52476–52484. https://doi.org/10.1039/C4RA08418G
Minsoo S et al (2008) Microstructure and properties of polyamideimide/silica hybrids compatibilized with 3-aminopropyltriethoxysilane. J Eur Polym 44:2236–2243. https://doi.org/10.1016/j.eurpolymj.2008.04.037
Miola M, Perero S, Ferraris S, Battiato A, Manfredotti C, Vittone E et al (2014) Silver nanocluster-silica composite antibacterial coatings for materials to be used in mobile telephones. Appl Surf Sci 313:107–115. https://doi.org/10.1016/j.apsusc.2014.05.151
Moulder JF, Stickle WF, Sobol PE, Bomben KD (eds) (1992) Hand book of X-ray photoelectron spectroscopy. Perkin-Elmer Corporation, Physical Electronics Division, Eden Prairie
NIST (2012) X-ray Photoelectron Spectroscopy Database, Version 4.1, National Institute of Standards and Technology, Gaither-burg. http://srdata.nist.gov/xps/
Nivethaa EAK, Narayanan V, Stephen A (2015) Synthesis and spectral characterization of silver embedded chitosan matrix nanocomposite for the selective colorimetric sensing of toxic mercury. Spectrochim Acta Part A Mol Biomol Spectrosc 143:242–250. https://doi.org/10.1016/j.saa.2015.01.075
Ohtsuki C, Ichikawa Y, Shibata H, Kawachi G, Torimoto T, Ogata S (2010) Sensing of protein adsorption with a porous bulk composite comprising silver nanoparticles deposited on hydroxyapatite. J Mater Sci Mater Med 21:1225–1232. https://doi.org/10.1007/s10856-009-3982-z
Penkova A, Blanes JMM, Cruz SA, Centeno MA, Hadjiivanov K, Odriozola JA (2009) Gold nanoparticles on silica monospheres modified by amino groups. Microporous Mesoporous Mater 117:530–534. https://doi.org/10.1016/j.micromeso.2008.07.041
Rabiej M (2014) A hybrid immune-evolutionary strategy algorithm for the analysis of the wide-angle X-ray diffraction curves of semicrystalline polymers. J Appl Crystallogr 47:1502–1511. https://doi.org/10.1107/s1600576714014782
Ren MQ, Jin YK, Chen WT, Huang WX (2015) Rich capping ligand–Ag colloid interactions. J Phys Chem C 119:27588–27593. https://doi.org/10.1021/acs.jpcc.5b09958
Ruozi B, Belletti D, Vandelli MA, Pederzoli F, Veratti P (2014) AFM/TEM complementary structural analysis of surface-functionalized nanoparticles. J Phys Chem Biophys 4:150–157. https://doi.org/10.4172/2161-0398.100015
Sakura T, Takahashi T, Kataoka K, Nagasaki Y (2005) One-pot preparation of mono-dispersed and physiologically stabilized gold colloid. Colloid Polym Sci 284:97–101. https://doi.org/10.1007/s00396-005-1339-9
Sarathy KV, Kulkarni GU, Rao CNR (1997) A novel method of preparing thiol-derivatised nanoparticles of gold, platinum and silver forming superstructures. Chem Commun 6:537–538. https://doi.org/10.1039/A700738H
Schon G (1973) ESCA studies of Ag, Ag_2O and AgO. Acta Chem Scand 27:2623–2633. https://doi.org/10.3891/acta.chem.scand.27-2623
Sharma VK, Yngard RA, Lin Y (2009) Silver nanoparticles: green synthesis and their antimicrobial activities. Adv Coll Interface Sci 145:83–96. https://doi.org/10.1016/j.cis.2008.09.002
Sing KSW, Everett DH, Haul RAW, Moscou L, Pierotti RA, Rouquerol J et al (1985) Reporting physisorption data for gas solid systems with special reference to the determination of surface-area and porosity (recommendations 1984). Pure Appl Chem 57:603–619. https://doi.org/10.1351/pac198557040603
Sohaebuddin SK, Thevenot PT, Baker D, Eaton JW, Tang LP (2010) Nanomaterial cytotoxicity is composition, size, and cell type dependent. Part Fibre Toxicol. https://doi.org/10.1186/1743-8977-7-22
Stenkamp VS, McGuiggan P, Berg JC (2001) Restabilization of electrosterically stabilized colloids in high salt media. Langmuir 17:637–651. https://doi.org/10.1021/la001086c
Suzuki TM, Nakamura T, Fukumoto K, Yamamoto M, Akimoto Y, Yano K (2008) Direct synthesis of amino-functionalized monodispersed mesoporous silica spheres and their catalytic activity for nitroaldol condensation. J Mol Catal A Chem 280:224–232. https://doi.org/10.1016/j.molcata.2007.11.012
Thompson DG, Enright A, Faulds K, Smith WE, Graham D (2008) Ultrasensitive DNA detection using oligonucleotide-silver nanoparticle conjugates. Anal Chem 80:2805–2810. https://doi.org/10.1021/ac702403w
Turci F, Ghibaudi E, Colonna M, Boscolo B, Fenoglio I, Fubini B (2010) An integrated approach to the study of the interaction between proteins and nanoparticles. Langmuir 26:8336–8346. https://doi.org/10.1021/la904758j
Uchihara T (2007) Silver diagnosis in neuropathology: principles, practice and revised interpretation. Acta Neuropathol 113:483–499. https://doi.org/10.1007/s00401-007-0200-2
Wang QQ, Shantz DF (2010) Nitroaldol reactions catalyzed by amine-MCM-41 hybrids. J Catal 271:170–177. https://doi.org/10.1016/j.jcat.2010.01.010
Wang YA, Li JJ, Chen HY, Peng XG (2002) Stabilization of inorganic nanocrystals by organic dendrons. J Am Chem Soc 124:2293–2298. https://doi.org/10.1021/ja016711u
Wang DJ, Xue GL, Zhen YZ, Fu F, Li DS (2012) Monodispersed Ag nanoparticles loaded on the surface of spherical Bi_2WO_6 nanoarchitectures with enhanced photocatalytic activities. J Mater Chem 22:4751–4758. https://doi.org/10.1039/c2jm14448d
Weaver JF, Hoflund GB (1994) Surface characterization study of the thermal-decomposition of AgO. J Phys Chem 98:8519–8524. https://doi.org/10.1021/j100085a035
Weisbecker CS, Merritt MV, Whitesides GM (1996) Molecular self-assembly of aliphatic thiols on gold colloids. Langmuir 12:3763–3772. https://doi.org/10.1021/la950776r
Wolan JT, Hoflund GB (1998) Surface characterization study of AgF and AgF_2 powders using XPS and ISS. Appl Surf Sci 125:251–258
Yang WJ, Neoh KG, Kang ET, Teo SLM, Rittschof D (2013) Stainless steel surfaces with thiol-terminated hyperbranched polymers for functionalization via thiol-based chemistry. Polym Chem 4:3105–3115. https://doi.org/10.1039/c3py00009e
Yeo SY, Lee HJ, Jeong SH (2003) Preparation of nanocomposite fibers for permanent antibacterial effect. J Mater Sci 38:2143–2147. https://doi.org/10.1023/a:1023767828656
Zhang JP, Chen P, Sun CH, Hu XJ (2004) Sonochemical synthesis of colloidal silver catalysts for reduction of complexing silver in DTR

system. Appl Catal A Gen 266:49–54. https://doi.org/10.1016/j.apcata.2004.01.025

Zhang WZ, Qiao XL, Chen JG, Wang HS (2006) Preparation of silver nanoparticles in water-in-oil AOT reverse micelles. J Colloid Interface Sci 302:370–373. https://doi.org/10.1016/j.jcis.2006.06.035

Zhang JF, Chen Y, Brook MA (2013) Facile functionalization of PDMS elastomer surfaces using thiol ene click chemistry. Langmuir 29:12432–12442. https://doi.org/10.1021/la403425d

Zhao Y, Perez-Segarra W, Shi QC, Wei A (2005) Dithiocarbamate assembly on gold. J Am Chem Soc 127:7328–7329. https://doi.org/10.1021/ja050432f